Swiss Journal of Palaeontology

RESEARCH

Open Access

A new tubalepid fish (Antiarcha, Placodermi) from the Middle Devonian of Huize, Yunnan, China

Yanchao Luo[1,2], Zhaohui Pan[1] and Min Zhu[1,2*]

Abstract

A new genus and species of tubalepid antiarch, *Tongdulepis concavus* gen. et sp. nov., is described from the Middle Devonian (Qujing Formation, late Eifelian) in Huize County, Qujing, northeastern Yunnan, China. It differs from other antiarchs in the trapezoidal premedian plate, the absence of a postmarginal plate (except *Tubalepis*), trifid preorbital recess, contorted infraorbital sensory line on the lateral plate, and an anterior median dorsal plate with broad anterior margin and concave posterior margin. This material confirms the absence of the postmarginal plate in Tubalepididae and adds to the understanding of the neurocranium and brachial process in basal bothriolepidoids. Our phylogenetic result places *Tongdulepis* gen. nov. within Tubalepididae, specifically at the plesiomorphic position of the *Tenizolepis-Dianolepis-Bothriolepis* lineage.

Keywords Antiarcha, Tubalepididae, Middle Devonian, Phylogeny, China

Introduction

Placoderms (armored fishes) are the most diverse fish group (jawed stem-Gnathostomata) that existed during the Silurian and Devonian periods, which is also known as the 'Age of Fishes' (Young, 2010). Antiarcha, one of the main groups among placoderms, is represented by three subgroups: Yunnanolepidoidei, Sinolepidoidei, and Euantiarcha (Denison, 1978; Janvier, 1995; Pan et al., 2018; Ritchie et al., 1992; Wang & Zhu, 2018; Zhu, 1996). Their morphological disparities are often based on the changes in the skull proportion, trunk armor pattern, development of the pectoral appendage, and its articulation with the trunk shield (Denison, 1978; Downs et al., 2019; Newman et al., 2019). However, unlike Arthrodira, a more crownward placoderm group, Antiarcha showed few disparities in the skull roof pattern. Though their contour may change, the skull roofs of different antiarch groups have all shown the same component bones, consisting of a premedian plate, a rostral plate, a pineal plate, a postpineal plate, a nuchal plate, and paired lateral plates, postmarginal plates, and paranuchal plates.

Moloshnikov (2011) established the family Tubalepididae for *Tubalepis* (Panteleyev & Moloshnikov, 2003; Sergienko, 1961), from the Upper Devonian of Krasnoyarsk, Kazakhstan, based on a paranuchal plate that lacks the anterolateral margin, and other features. He suggested that *Tubalepis* might have lost its postmarginal plate, representing the first antiarch that changed its skull roof composition. However, due to the rarity of head shield material, the absence of a postmarginal plate in *Tubalepis* remained uncertain. Although the phylogenetic position of Antiarcha has received attention for decades, most of the previous studies placed Antiarcha as the most basal group of Placodermi or the jawed stem-gnathostomes (Brazeau, 2009; Carr

Handling editor: Torsten Scheyer

*Correspondence:
Min Zhu
zhumin@ivpp.ac.cn
[1] Key Laboratory of Vertebrate Evolution and Human Origins of Chinese Academy of Sciences, Institute of Vertebrate Paleontology and Paleoanthropology, Chinese Academy of Sciences, Beijing 100044, China
[2] University of Chinese Academy of Sciences, Beijing 100049, China

et al., 2009; Goujet & Young, 1995; Qiao et al., 2016; Zhu et al., 2013, 2021, 2022). The homology of the plates between antiarchs and some other placoderms, like *Kujdanowiaspis* (Dupret, 2010; Dupret et al., 2017; Stensiö, 1942) and *Romundina* (Goujet & Young, 2004), is acknowledged. The postmarginal plates in Antiarcha and Arthrodira often occupy the lateral sides of their skull roofs and form the lateral corners. Most basal antiarchs tend to bear a branch from the principal section of the infraorbital sensory line on the lateral plate, which often extends to the postmarginal plate (preopercular sensory line), as in other basal placoderms (Young & Zhang, 1996; Zhang, 1980).

During fieldwork in 2021, we discovered a new vertebrate fossil site in the Middle Devonian (the lowermost part of the Qujing Formation, late Eifelian) of Luna Township, Huize County, Qujing, Yunnan, China (Fig. 1). The fauna includes onychodonts, tetrapodomorphs, dipnoans (Luo et al., 2022), and placoderms. Here, we describe *Tongdulepis concavus* gen. et sp. nov. from this fossil site, based on a well-preserved specimen with head shield, trunk armor, and articulated pectoral appendages. This well-preserved fossil supports the diagnosis of Tubalepididae and enhances our understanding of plesiomorphic bothriolepidoids. Interesting features from *Tongdulepis* gen. nov., such as the wide orbital fenestra, more vertical pectoral appendages, and ridge-less trunk armor lacking a regular median ventral plate, delineate Tubalepididae as a distinct group within Bothriolepidoidei.

Material and methods

Material

The holotype of *Tongdulepis concavus* gen. et sp. nov. (IVPP V33248) was collected from the calcareous mudstone of the Qujing Formation at Huize in Qujing City, Yunnan Province, China (Luo et al., 2022). It is currently housed at the IVPP. The specimen was CT-scanned with the GE v|tome|x m300&180 micro-computed tomography scanner from the Key Laboratory of Vertebrate Evolution and Human Origins of the Chinese Academy of Sciences. The scan had a resolution of 38.823 μm and was conducted at 180 kV/100 mA. The images were optimized and converted using VGStudio Max v.3.0, and the optimization and further reconstruction were completed in Mimics v.18.01. The Nikon D3X camera was used to take photographs of *Tongdulepis* gen. nov. All the measurements were done in Mimics. The sizes in the axial direction (from head to tail) are referred to as length, and the sizes in the transverse direction (from pectoral appendage to pectoral appendage) are referred to as width.

Phylogeny

To explore the phylogeny of *Tongdulepis* gen. nov. among the antiarchs, we compiled a matrix (see 'Supplementary Materials') using Mesquite V.3.61 (Maddison & Maddison, 2019). Our phylogenetic analysis was conducted in TNT v.1.5 (Goloboff & Catalano, 2016). The matrix herein primarily follows the works of Young (1984b, 1988), Zhu (1996), Ritchie et al. (1992), Wang and Zhu (2018), and Plax and Lukševičs (2023), while also

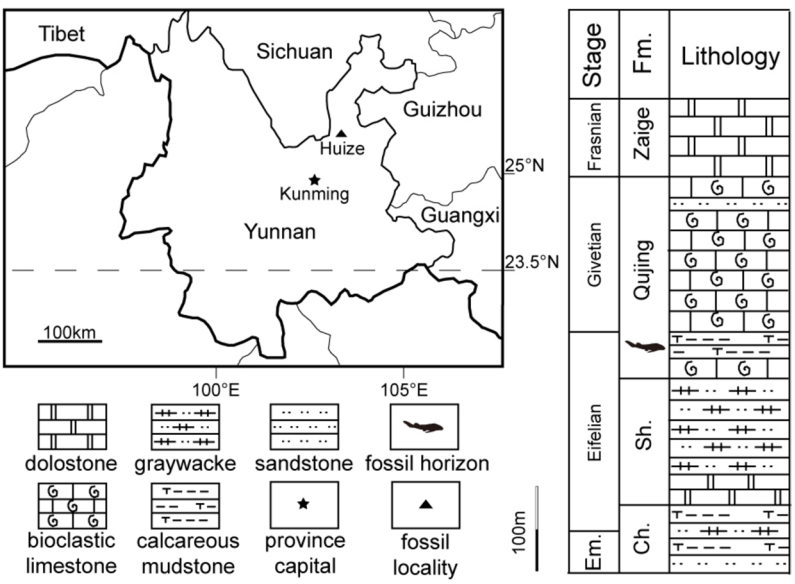

Fig. 1 Map of the locality site and the fish-bearing horizon in this study

introducing new taxa and substituting genera with species as the smallest Operational Taxonomic Unit (OTU) to facilitate a more in-depth analysis. We incorporated 51 ingroup taxa and 11 new characters (Ch. 81–91) that had not been included in previous parsimony analyses. Our comprehensive matrix comprises 2 outgroup taxa (*Kujdanowiaspis* and *Romundina*), 85 ingroup taxa, and 92 characters (with Ch. 18, 48, and 49 designated as ordered). For a more resolved result, we excluded taxa with completeness lower than 40%, leaving 46 ingroup taxa in our final matrix (see 'Supplementary Materials').

Systematic paleontology

Class Placodermi McCoy, 1848

Order Antiarcha Cope, 1885

Suborder Euantiarcha Janvier & Pan, 1982

Infraorder Bothriolepidoidei Miles, 1968

Family Tubalepididae Moloshnikov, 2011

Tongdulepis gen. nov.

Type and only species—Tongdulepis concavus sp. nov.

LSID: urn:lsid:zoobank.org:act:DC6ECD27-4858-41CC-AAFB-7524C16ACCA9.

Etymology—The generic name '*Tongdu-*' is after the epithet of Huize County, which means 'The Copper City' in Chinese. People from Huize started copper mining and smelting in the twelfth century BC and invented the cupronickel by the third century AD. The copper industry of Huize funded the Chinese dynasties till the end of the Feudal Age.

Diagnosis—A middle-sized tubalepid antiarch resembling *Tubalepis* in tubercular ornamentation, anterior median dorsal plate with wide anterior margin, absence of postmarginal plate, and elongated trunk shield. It can be distinguished by the following combination of characters: isosceles trapezoidal premedian plate; trifid preorbital recess; contorted infraorbital sensory lines on lateral plates; nuchal plate without orbital facets; wide and narrow orbital fenestra; anterior median dorsal plate overlapping mixilateral plates; anterior median dorsal plate with concave posterior margin; ridge-less trunk armor; large axillary foramen.

Remarks—Moloshnikov (2011) established the family Tubalepididae, designating *Tubalepis* as the type genus. Considering that the skull of *Tubalepis* is currently known only from a paranuchal plate, the skull features attributed to *Tongdulepis* gen. nov. cannot be regarded as the characteristics of Tubalepididae, as they may or may not be present in *Tubalepis*. Additional skull material of *Tubalepis* is needed to clarify these characteristics.

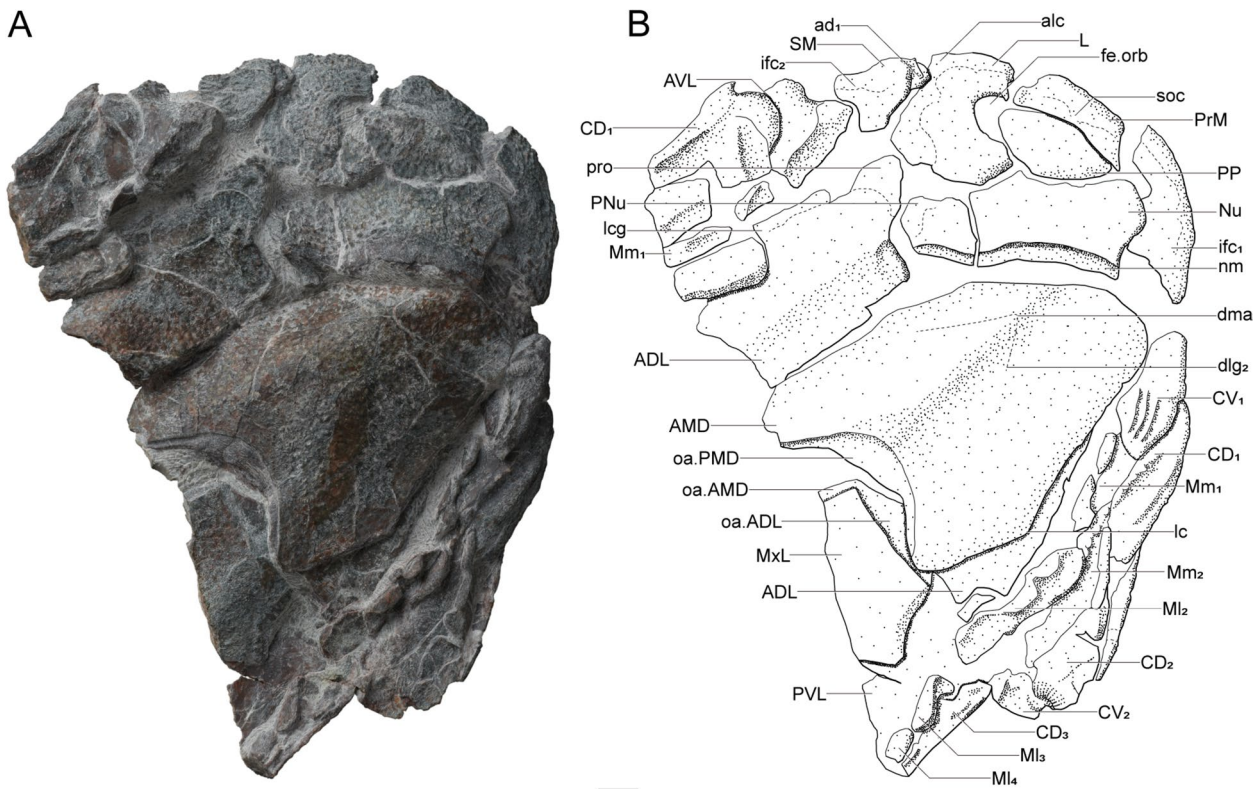

Fig. 2 Holotype of *Tongdulepis concavus* gen. et sp. nov. (IVPP V33248) in dorsal view. **A** photograph; **B** interpretive drawing. Scale bar = 10 mm

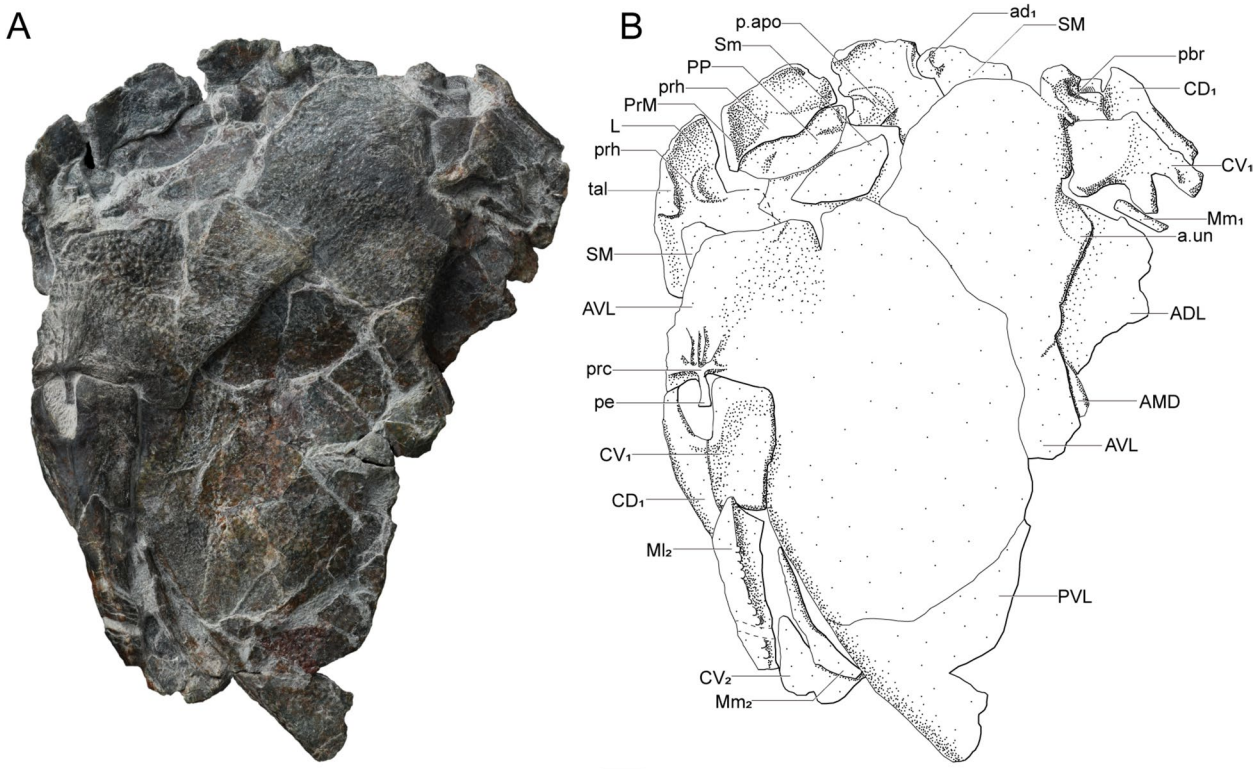

Fig. 3 Holotype of *Tongdulepis concavus* gen. et sp. nov. (IVPP V33248) in ventral view. **A** photograph; **B** interpretive drawing. Scale bar = 10 mm

Tongdulepis concavus sp. nov.

Figures 2, 3, 4, 5, 6, 7C, D

Etymology—The specific epithet '*concavus*' refers to the highly concave posterior margin of the anterior median dorsal plate.

Diagnosis—As for the genus.

Holotype—IVPP V33248, a flattened individual with head shield, trunk armor, and pectoral appendages.

Type locality and horizon—Luna, Huize County, northeastern Yunnan Province, China; Qujing Formation; late Eifelian, Middle Devonian (Fig. 1).

Description

General features

The holotype (IVPP V33248) comprises an almost complete head shield, trunk armor, and pectoral appendages. Its surface is covered with sporadic and shallow tubercular ornamentation. The posterior median dorsal and median ventral plates are missing, and the mixilateral and posterior ventrolateral plates, as well as the distal segment of the pectoral appendage, are incomplete. The entire fossil has undergone extensive recrystallization, resulting in unsatisfactory CT scanning outcomes.

Head shield

Premedian plate—The premedian plate (PrM, Figs. 2, 3, 4, 7c) is isosceles trapezoidal in shape, short and broad. Its rostral margin is 31.6 mm wide, and the orbital margin of the PrM plate is slightly convex and measures 48.3 mm in width. The PrM plates of other antiarchs are typically inverted trapezoidal or fan-shaped, with their rostral margins mostly greater than or equal to the orbital margins. The trapezoidal PrM plate in *Tongdulepis* gen. nov. may be apomorphic compared with *Microbrachius* (Fig. 7A; Hemmings, 1978), which also has an introvertive part of the lateral margin of the PrM plate. Besides, the length of the PrM plate in *Tongdulepis* gen. nov. is 11.3 mm, which is longer than that of the lateral plates, suggesting that the PrM may protrude from the rostral margin of the head shield (Figs. 2, 3, 4). The contorted principal section of the infraorbital sensory line on the head shield (ifc_1, Figs. 2B, 4B, 7B) extends from the lateral plate (L, Figs. 2B, 3B, 4) to the PrM plate, and the anterior section of the supraorbital sensory line (soc, Figs. 2B, 4B) is shallow. On the visceral surface of the PrM plate, a preorbital recess (prh, Figs. 3B, 4D) reaches anteriorly to the center of the PrM plate and extends aside to the L plates.

Lateral plate—The paired L plates (Figs. 2, 3, 4, 7c) contact the lateral margins of the PrM plate. The

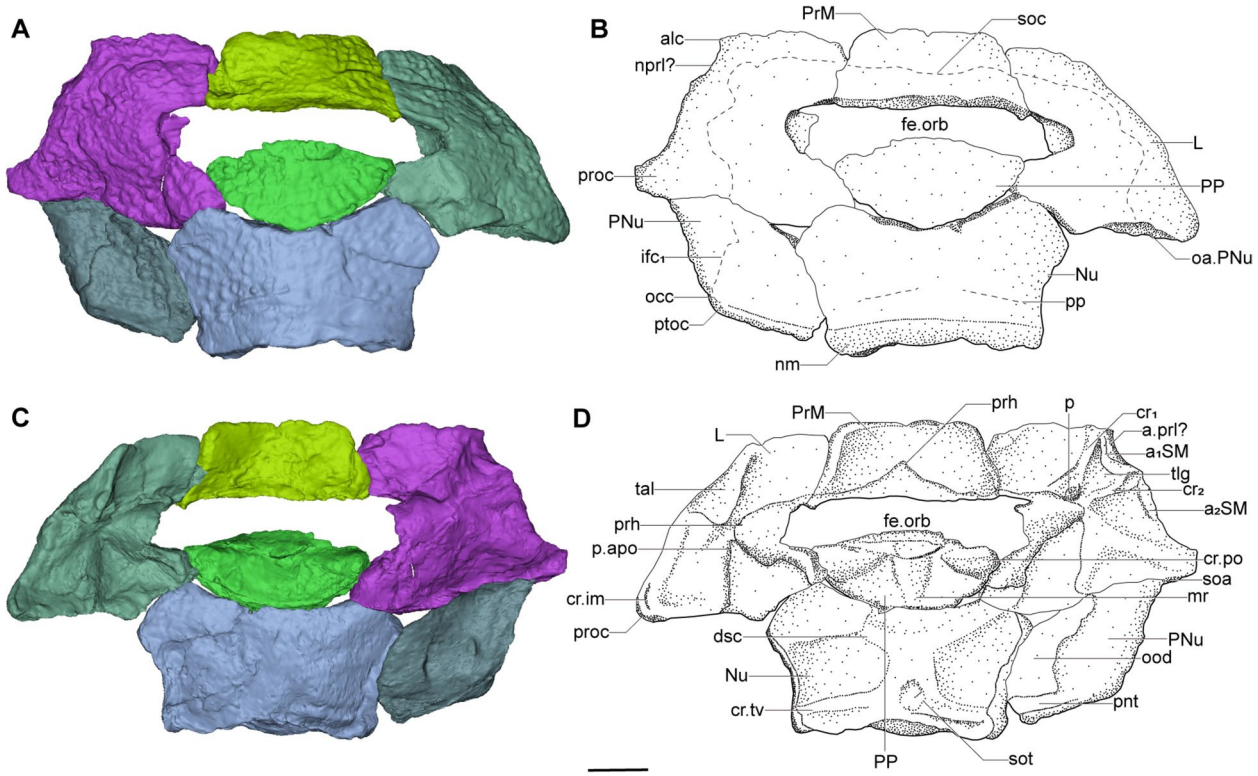

Fig. 4 The three-dimensional reconstruction of the head shield of *Tongdulepis* gen. nov. **A** virtual rendering in dorsal view; **B** interpretive drawing in dorsal view; **C** virtual rendering in visceral view; **D** interpretive drawing visceral view. Scale bar = 10 mm

complete left plate is 31.0 mm wide and 32.7 mm long, with the anterolateral angle of the head shield (alc, Figs. 2B, 4B) on its anterolateral corner. The contorted infraorbital sensory line runs across the dorsal surface of the L plate and extends to the PrM plate. On the anterolateral margin of the right L plate, a deltoid-shaped thickening (tal, Figs. 3B, 4D) occupies the notch between the PrM and the right L plate. It shares topological similarities with the prelateral plates in *Bothriolepis* (Béchard et al., 2014; Young, 1984c, 1988), *Grossilepis* (Lukševičs, 2001; Miles, 1968; Olive, 2015; Stensiö, 1948), and *Nawagiaspis* (Young, 1990). The branch of the infraorbital sensory line (ifc_2, Figs. 2B, 4B) in *Tongdulepis* gen. nov. is absent on this thickening but extends directly to the submarginal plate (SM, Figs. 2B, 3B). Considering the branch of the infraorbital sensory line in other antiarchs primarily extending to the prelateral plate (Young, 2008; Young & Zhang, 1996) and the possible prelateral notch (nprl?, Fig. 4B) at the corresponding position of the left L plate, we suggest with caution that the thickening might be a fused prelateral plate. An overlap area on the posterior margin of the right L plate indicates the suture morphology between the L plate and the paranuchal plate (PNu, Figs. 2B, 4).

On the visceral side of the L plate, the preorbital recess extends from the PrM plate and surrounds the orbital fenestra (fe.orb, Fig. 4). The preorbital recess on the L plate is semicircular. Together with the middle part on the PrM, the preorbital recess in total is trifid, as seen in some *Bothriolepis* species (Young, 1988). The middle part of the preorbital recess on the PrM plate is similar to that of *Wudinolepis* (Zhang, 1965). Still, the flank part of the preorbital recess extends to the lateral margin as *Jiangxilepis* (Zhang & Liu, 1991), which may be a transitional feature. A narrow plane near the anterolateral corner of the head shield may represent the attachment area for the prelateral plate (a.PrL?, Fig. 4D). A triangular transverse lateral groove of the head shield (tlg, Fig. 4D) is outlined by the prelateral and posterolateral cristae ($cr_{1\text{-}2}$, Fig. 4D) next to the attachment area. The lateral pit (p, Fig. 4D) is anteromedial of the transverse lateral groove, just in front of the lateral lobe of the preorbital recess, and much smaller than that of *Bothriolepis* (Luo et al., 2023; Young, 1988). The anterior postorbital process (p.apo, Figs. 3B, 4D) extends anteriorly to the level of the orbital notch (between the posterior margin and the anterior margin of the orbital fenestra) and is close to the posterior of the preorbital recess. The anterior attachment area for the submarginal plate (a_1SM, Fig. 4D) is anterolateral of the

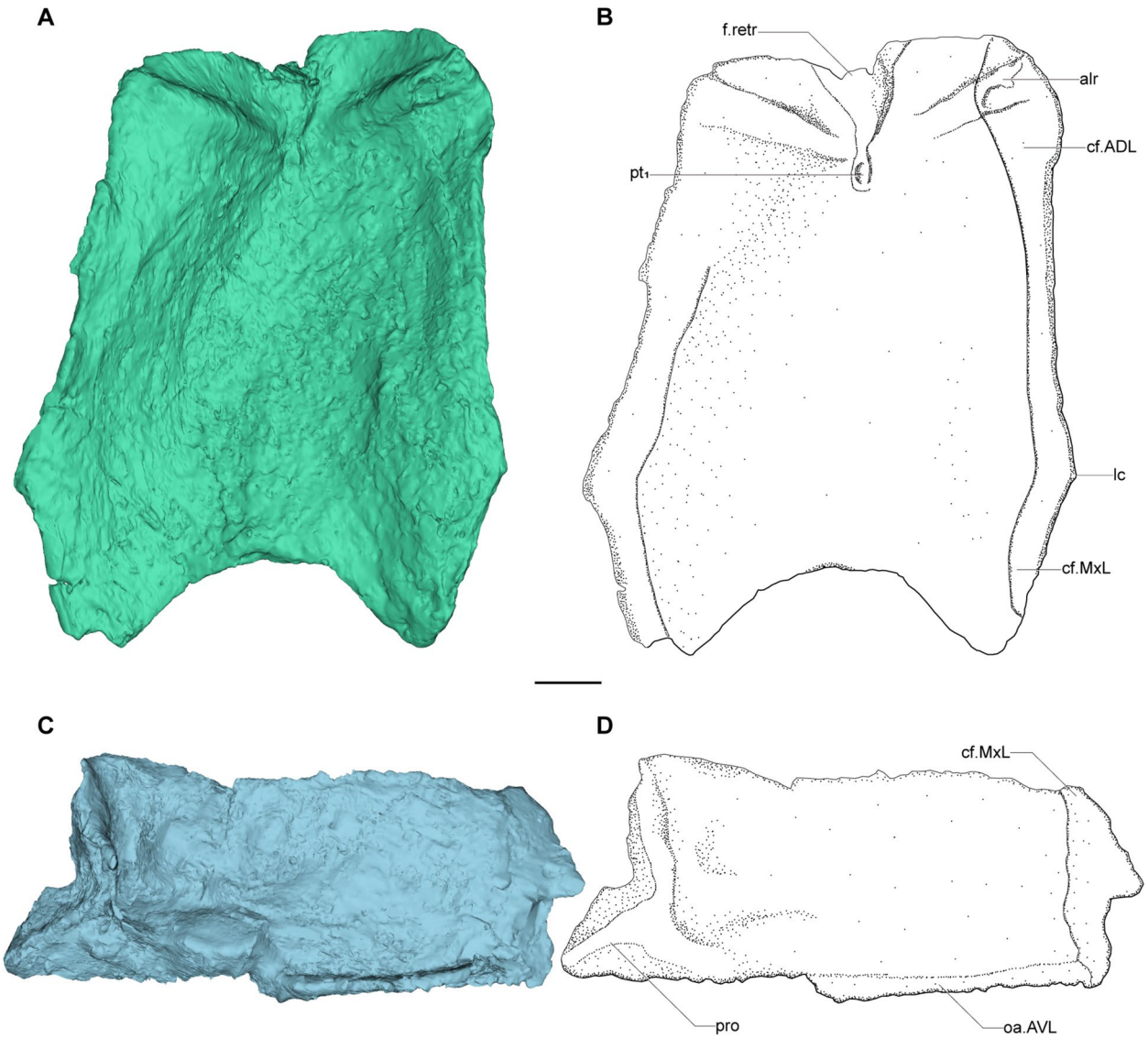

Fig. 5 The three-dimensional reconstruction of the trunk plates of *Tongdulepis* gen. nov. in visceral view. **A** virtual rendering of the AMD plate; **B** interpretive drawing of the AMD plate; **C** virtual rendering of the right ADL plate; **D** interpretive drawing of the right ADL plate. Scale bar = 10 mm

transverse lateral groove and connects the anterior articular process of the SM plate (ad_1, Figs. 2B, 3B). The posterior attachment area for the submarginal plate (a_2SM, Fig. 4D) is short and occupies less than one-third of the lateral margin between the posterolateral cristae and the preobstantic corner (proc, Fig. 4). The posterior attachment area in the bothriolepid lineage mainly extends from the anterior attachment area to the lateral end of the L plate. Because the postmarginal plate is absent, the depressions of the inframarginal crista (cr.im, Fig. 4D) and the subobstantic area (soa, Fig. 4D) are also located on the visceral side of the L plate.

Postpineal plate—The postpineal plate (PP, Figs. 2, 3, 4, 7C) is 13.8 mm long and has a maximum width of 30.2 mm. Its anterior margin is convex and protrudes into the orbital fenestra, which extends two-thirds of the width of the head shield (Figs. 4, 7B). Its lateral margin contacts the L plates. On the visceral side of the PP plate, paired postorbital cristae (cr.po, Fig. 4D) are developed. They are approximately transverse, each occupying one-third of the PP plate's width. Because the developed preorbital recess nearly surrounds the orbital fenestra, the postorbital cristae meet the preorbital recess on the L plates at the lateral margins of the PP plate. A broad and gradually

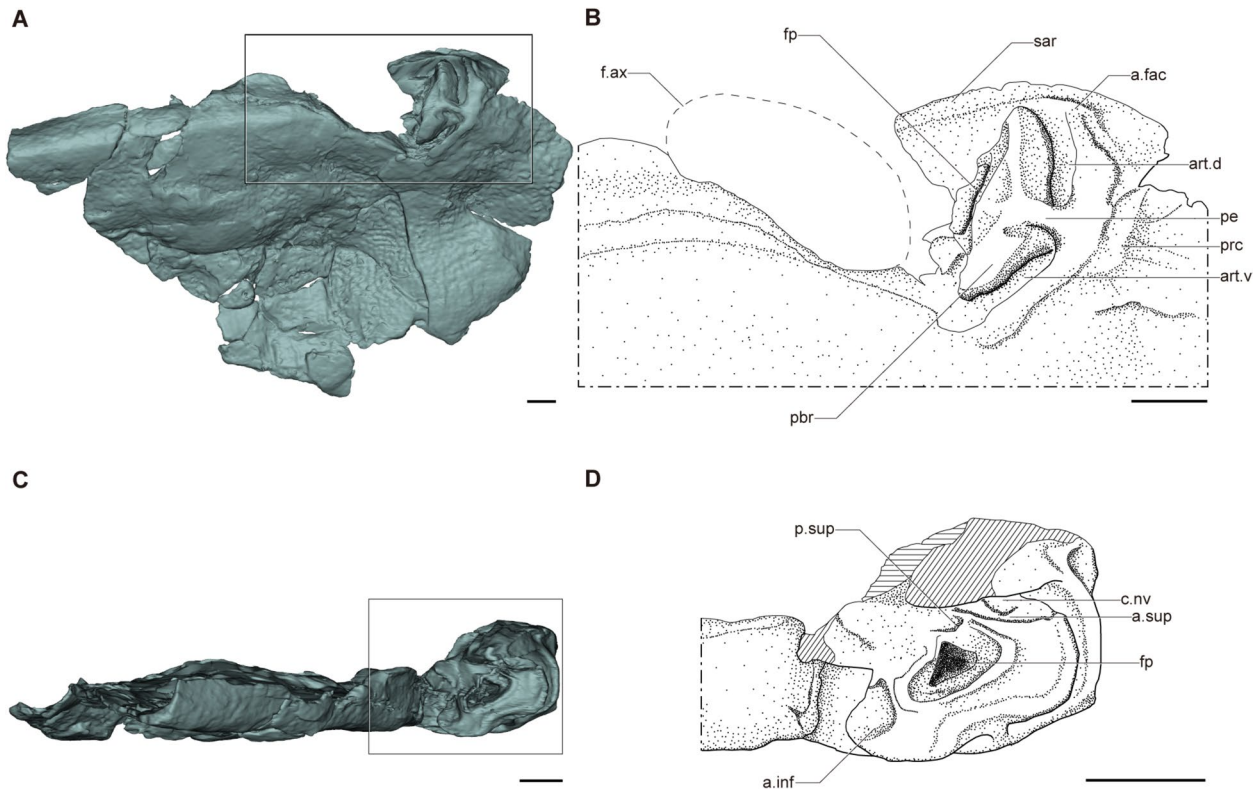

Fig. 6 The three-dimensional reconstruction of the right brachial process of *Tongdulepis* gen. nov. **A** virtual rendering in ventrolateral view; **B** interpretive drawing in ventrolateral view; **C** virtual rendering in posterior view; **D** interpretive drawing in posterior view. The interlaced lines mark the fractured surfaces. Scale bars = 10 mm

narrowing median ridge (mr, Fig. 4D) is between these postorbital cristae.

Nuchal plate—The nuchal plate (Nu, Figs. 2, 4, 7C) is measured at 42.9 mm wide and 24.1 mm long, and contacts the posterior margin of the PP plate. The posterior pit line grooves (pp, Fig. 4B) run posterolaterally through the dorsal surface of the Nu plate. The obtected nuchal area of the head shield (nm, Figs. 2B, 4B) is on the posterior margin of the Nu plate and extends laterally to the PNu plates (Figs. 2B, 4B). The obtected area is relatively deep, suggesting a stronger connection between the head and trunk shields. The available specimens of *Tubalepis* and the dianolepids often lack evidence of the neurocranium, which is presumed to be present but not preserved. Our reconstruction of the head shield reveals some transitional features between the neurocrania of the bothriolepids and plesiomorphic antiarchs. The visceral side of the Nu plate (Fig. 4C, D) is relatively flattened, and mainly occupied by the otico-occipital depression (ood, Fig. 4D). The depressions caused by the semicircular canals (dsc, Fig. 4D) are shallow, and the anterior portion of the semicircular canal of *Tongdulepis* gen. nov. is less oblique than in the bothriolepids (Wang & Zhu, 2018). The supraotic thickening (sot, Fig. 4D) of *Tongdulepis* gen. nov. is small and posterior, while that of the bothriolepids is often large and on the center of the Nu plate (Luo et al., 2023; Wang & Zhu, 2018; Young, 1983). The transverse nuchal crista (cr.tv, Fig. 4D) runs through the posterior margin of the Nu plate with a continuous posterior margin, without the extended posterior process and median occipital crista in the bothriolepids (Wang & Zhu, 2018).

Paranuchal plate—Only the left PNu plate is preserved (Figs. 2, 4, 7C). It is measured at 21.2 mm wide and 14.3 mm long. Like *Tubalepis*, it lacks the anterolateral margin found in other antiarchs. Its mesial and anterior margins only contact the L and Nu plates. The shape of the PNu plate in *Tubalepis* (Moloshnikov, 2011) led Moloshnikov to presume there was no postmarginal plate in *Tubalepis*. On that basis, he established the family Tubalepididae. The material of *Tongdulepis* gen. nov. supports Moloshnikov's opinion. Accordingly, the preobstantic corner of the head shield is formed instead by the L plate. The infraorbital sensory line that extends from the L plate goes through the dorsal surface of the PNu plate and diverges a short segment of the occipital cross commissure (occ, Fig. 4D) near the posterolateral margin

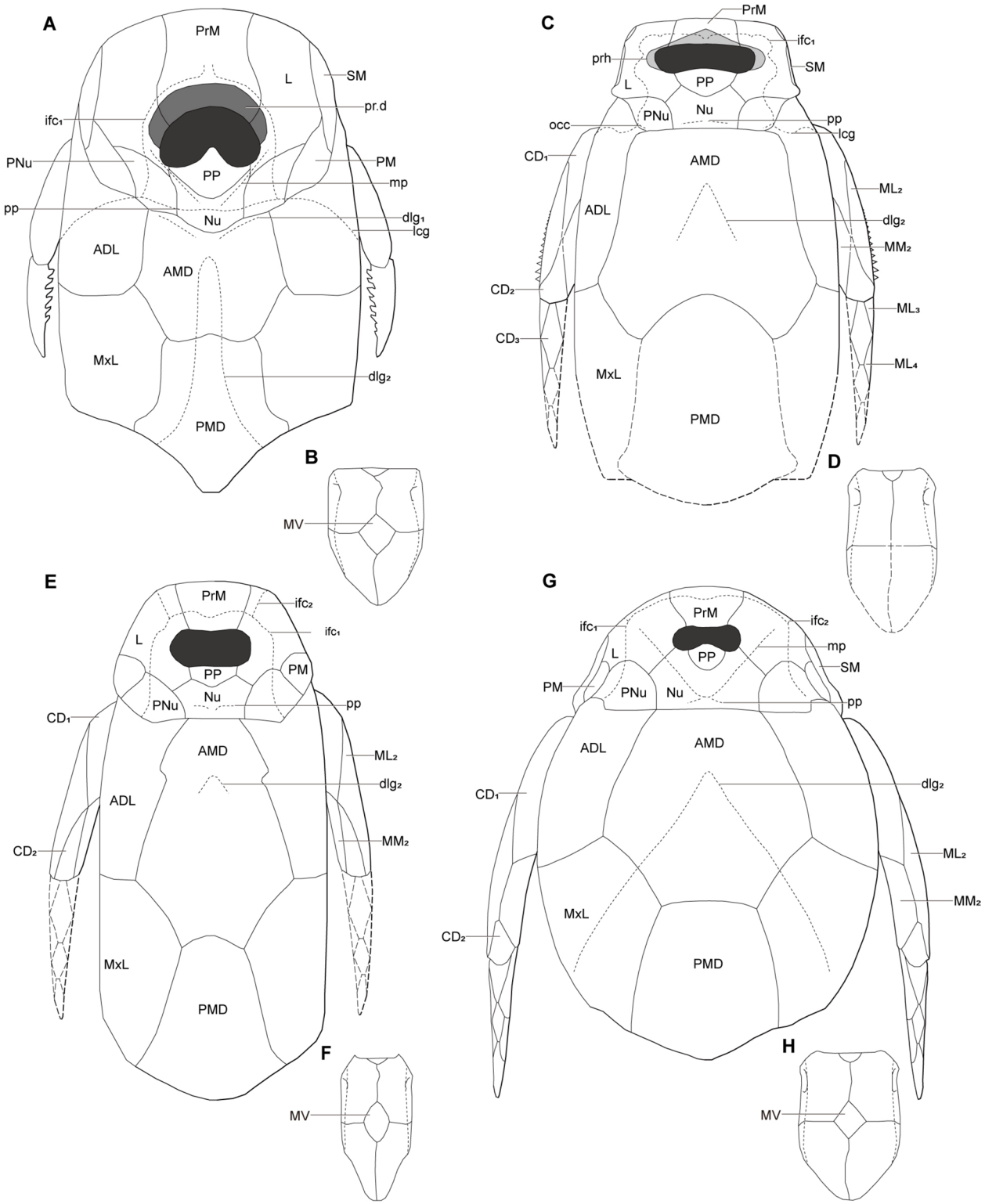

Fig. 7 Comparison of head and trunk shields of several bothriolepidoid representatives. **A**, **B** *Microbrachius* in dorsal (**A**) and ventral (**B**) views; **C**, **D**, *Tongdulepis* gen. nov. in dorsal (**C**) and ventral (**D**) views; **E–F**, *Tenizolepis* in dorsal (**E**) and ventral (**F**) views; **G**, **H**, *Bothriolepis* in dorsal (**G**) and ventral (**H**) views. **A** redrawn from Long et al. (2015), B redrawn from Wang and Zhang (1999), **E** and **F** redrawn from Moloshnikov (2011), **G** and **H** redrawn from Béchard et al. (2014). Not to scale

of the PNu plate. On the visceral side of the PNu plate, the otico-occipital depression (ood, Fig. 4D) is extensive and extends almost half the width of the PNu plate. The otico-occipital depression in other antiarchs (e.g., *Phymolepis* and *Bothriolepis*; Wang & Zhu, 2018; Luo et al., 2023) only occupies one-third of the anterior margins of the PNu plate. This difference is mainly caused by the variation in the size of the PNu plate, whereas the dimension of the otico-occipital depression remains constant. Many antiarchs tend to have the PNu plate that extends laterally to the same extent as the L plate (Fig. 7). By comparison, the PNu plate of *Tongdulepis* gen. nov. is narrow and does not extend laterally to the same extent as the L plate. The transverse nuchal crista on the Nu plate is continuous with the paranuchal trochlea (pnt, Fig. 4D). The crista and trochlea jointly form a roughened ridge that extends to the postobstantic corner of the head shield.

Cheek

Submarginal plate—The SM plate (Figs. 2, 3) is preserved only on the left side and is complete. It measures at 15.4 mm wide and 21.7 mm long, and contacts the lateral margin of the left L plate. Although the infraorbital sensory line is absent on the L plate, the sensory line is preserved ventrally onto the SM plate (Fig. 2B). A well-developed anterior articular process (ad_1, Figs. 2B, 3B) is on the anteromesial margin of the SM plate like the bothriolepids (Stensiö, 1948; Young, 1988). The posterior articular process is lost, undeveloped, or not preserved.

Trunk armor

Anterior median dorsal plate—The anterior median dorsal plate (AMD, Figs. 2, 5A, B, 7C) is a hexagon, about 71.9 mm wide and 81.3 mm long (length approximately 1.13 times the width). The index between the width of the anterior margin to the maximum width of the AMD plate is about 0.56, and the length index between the anterior and posterior divisions is about 2.07. The posterior oblique dorsal sensory line grooves (dlg_2, Fig. 2B) are anteriorly placed on the AMD, marking the tergal angle of the trunk armor (dma, Fig. 2B) and the anterior ventral pit (pt_1, Fig. 5B) on its visceral side. The AMD plate resembles *Tubalepis* in overall shape, with the wide anterior margin and the posteriorly positioned lateral corners (lc, Figs. 2B, 5B). The AMD plate of *Tongdulepis* gen. nov. bears a strong postlevator thickening (alr, Fig. 5B) and a much slender levator fossa (f.retr, Fig. 5B). It lacks the postnuchal notch, which is present in the bothriolepids (Moloshnikov, 2004, 2010; Olive, 2015; Young, 1983). *Tongdulepis* gen. nov. is also similar to *Grossilepis* (Olive, 2015) and *Asterolepis* (Newman et al., 2019) in the contact relationship between the AMD and surrounding plates. The visceral side of the AMD plate shows areas for overlapping the mixilateral and anterior dorsolateral plates (cf.MxL, cf.ADL, Fig. 5B). The AMD plate is overlapped by the posterior median dorsal plate (oa.PMD, Fig. 2B). The area overlapped by the PMD is 44.2 mm wide, suggesting a broad PMD plate with a notably convex anterior margin (Fig. 7B). Although the PMD plate of *Tongdulepis* gen. nov. is not preserved, its anterior margin can be inferred from the posterior margin of the AMD. The anterior margin of the PMD differs from that of other antiarchs, which typically exhibit a mildly convex anterior margin that does not extend anteriorly to the level of the lateral corner of the AMD (Lukševičs, 1991; Moloshnikov, 2012; Olive, 2015; Young, 1984a; Zhu, 1996).

Anterior dorsolateral plate—The left ADL plate (Figs. 2B, 3B, 7C) is 33.6 mm wide with posterior fractures, while the length of the complete right ADL plate is 87.5 mm (covered by the AMD plate, Figs. 5C, 5D). The dorsolateral ridge is poorly developed, indicating a smooth cross-section of the trunk shield. The obstantic process of the trunk armor (pro, Fig. 2B) extends anteriorly and articulates with the PNu plate, situated above the presumed gill opening. The length of the obstantic process is about half of the width of the ADL plate, similar to that of *Tubalepis* (Moloshnikov, 2012). By comparison, the obstantic process is short in some euantiarchs (e.g., *Bothriolepis* and *Tenizolepis*; Moloshnikov, 2012) or lacking in others (e.g., *Stegolepis*, *Sherbonaspis*, and *Kirgisolepis*; Malinovskaya, 1973; Young & Gorter, 1981; Panteleyev, 1992, 1993; Moloshnikov, 2011). The main lateral line groove (lcg, Fig. 2B) is on the ventral margin of the ADL plate and extends backward to its midpiece. The ADL plate overlaps the MxL plate posteriorly (cf.MxL, Fig. 5D) and is overlapped ventrally by the anterior ventrolateral plate (oa.AVL, Figs. 5D).

Mixilateral plate—Only part of the right MxL plate (Figs. 2B, 7C) is preserved (width 47.8 mm). The MxL plate is anteriorly and dorsolaterally overlapped by ADL and AMD plates (oa.ADL, oa.AMD, Fig. 2B). The overlapped area marks the connection between the MxL and ADL plates at the level of the lateral corner of the AMD plate and suggests the AMD plate overlapping the ADL and MxL plates.

Anterior ventrolateral plate—Both the anterior ventrolateral plates (AVL, Figs. 3, 6) are incomplete. The right AVL (72.5 mm wide, 113.2 mm long) overlaps the left as in most antiarchs (Jia et al., 2010; Lukševičs, 2001; Moloshnikov, 2008; Panteleyev & Moloshnikov, 2003; Ritchie et al., 1992). The incomplete lateral lamina of the AVL plate is 23.3mm in height. The remaining length of the right AVL plate exceeds twice the anterior margin of the head shield. The incomplete posterior part of the AVL plate has contact with the posterior ventrolateral plate

(PVL, Fig. 3B), and the area overlapping the median ventral plate is lacking, so the median ventral plate is either very small or absent.

Pectoral appendage articulation—The pectoral appendage articulation of *Tongdulepis* gen. nov. (Figs. 3, 6) is developed, but differs from the bothriolepids, showing the transformation in the euantiarchs. The prepectoral corner (prc, Figs. 3B, 6B) is undeveloped, placed anterior of the brachial process, anterolateral of the AVL plate. The pedal part of the brachial process (pe, Figs. 3B, 6B) is short and stout, which may limit the range of articulation. The insertion area for the abductor muscle, which is often observed in the bothriolepids (Lukševičs, 2001; Young, 1988; Young & Zhang, 1992), is missing in *Tongdulepis* gen. nov., suggesting a less flexible pectoral appendage. The short and straight dorsal and ventral articular depressions for the dermal processes of the pectoral appendage (art.d, art.v, Fig. 6) are placed nearly in a vertical line, which differs from the crescent articular depressions in the bothriolepids. This articular structure might also suggest constrained rotation ability in *Tongdulepis* gen. nov. The brachial process (pbr, Figs. 3B, 6) is helmet-shaped, but its orientation is distinctively pointed posteriorly, making the funnel pit (fp, Fig. 6) invisible in lateral view. The anterior dorsal and ventral muscle insertions (a.sup, a.inf, Fig. 6). Inside the anterior dorsal muscle insertion, a canal for nerves and/or vessels (c.nv, Fig. 6) is presented. The posterior dorsal muscle insertion (p.sup, Fig. 6) is aside from the anterior dorsal muscle insertion. Although the lateral lamina is incomplete, the ventral margin of the axillary foramen (f.ax, Fig. 6) is preserved posterior to the brachial process. The preserved margin (34.7 mm long) suggests a large axillary foramen, longer than the length of the brachial process. The axillary foramen tends to be smaller than the brachial process in most antiarchs (Young & Zhang, 1992), which would support more robust pectoral appendages in *Tongdulepis* gen. nov. A semicircular unornamented area (a.un, Fig. 3B) is on the ventral surface of the ADL plate, just below the axillary foramen.

Semilunar plate—The unpaired semilunar plate (Sm, Fig. 3B; 26.9 mm wide, 12.7 mm long) has a convex anterior margin. The Sm plate is fusiform and shapes a shallow notch on the AVL plates, similar to that of *Tenizolepis* (Moloshnikov, 2012) and *Tubalepis* (Panteleyev, 2001; Panteleyev & Moloshnikov, 2003).

Pectoral appendage—Both pectoral appendages are fragmented. The proximal segment of the left appendage includes disjoined dorsal and ventral central plates 1–2 ($CD_{1\text{-}2}$, $CV_{1\text{-}2}$, Figs. 2B, 3B, 7), lateral marginal plate 2 (Ml_2, Fig. 3B), and the mesial marginal plates 1–2 ($Mm_{1\text{-}2}$, Fig. 3B). The right proximal segment is distorted, but preserved with slightly more details. The proximal segment is thick, the length/width index is about 5. The CD_2 plate (Figs. 2B, 7C) extends anteriorly, and is restored with a narrow or point contact with the CD_1 (Fig. 7C). The right distal segment is incomplete and is comprised of the central plate 3 (CD_3, Figs. 2B, 7C) and fragments of the lateral marginal plate 3–4 ($Ml_{3\text{-}4}$, Fig. 2B).

Discussion

Phylogenetic analysis

The first comprehensive matrix analyzing the phylogeny of antiarchs was by Zhu (1996), expanding an initial matrix for Bothriolepidoidei by Zhang and Young (1992). Due to the diversity, convergences, and reversals in the evolution of Antiarcha, the interrelationships tend to be unstable. The matrix used here has been updated from recent analyses (Jia et al., 2010; Pan et al., 2018; Plax & Lukševičs, 2023; Wang & Zhu, 2018). Some definitions and codings are revised. The high diversity of antiarchs includes multiple species within a single genus. As such, the type species cannot represent polytropic characters of the genus, we have refined the ingroup taxa, replacing genera with species. We have coded 51 ingroup taxa not incorporated in previous phylogenetic analyses and added some new characters (Ch. 81–91). Our phylogenetic analysis yields 20 most parsimonious trees of length 270 steps (TBR), with a consistency index (CI) of 0.356, and a retention index (RI) of 0.718.

With additional characters provided by the new species, the result of our analysis improves previous understanding of Antiarcha (Fig. 8). The clade of *Chuchinolepis* (Node 1, Fig. 8) is characterized by the anterior postorbital process extending in front of the orbital notch (Ch. 35, state 1). Other yunnanolepidoids are placed into a clade (Node 2, Fig. 8) defined by the nerves and vessels to the pectoral fin passing through multiple axillary foramina (Ch. 91, state 0). The *Yunnanolepis-Parayunnanolepis-Mizia* lineage (Node 3, Fig. 8) is assembled by the internal posterior transverse crista of the trunk shield turning anteriorly and in front of posterior ventral process and pit (Ch. 60, state 1), and absence of the ventrolateral fossa of the trunk shield (Ch. 63, state 0). *Mizia* and *Parayunnanolepis* formed a monophyletic group (Node 4, Fig. 8), characterized by the absence of the postmarginal canal (Ch. 83, state 0).

Microbrachiidae is resolved as the sister group of the remaining euantiarchs (Node 5, Fig. 8), characterized by three synapomorphies: ridged ornamentation (Ch. 2, state 1); central sensory canal (Ch. 29, state 1); occipital cross-commissure long and extending onto nuchal plate (Ch. 34, state 1). *Microbrachius* (Node 6, Fig. 8) is defined by four synapomorphies: the subparallel ridges on dorsal

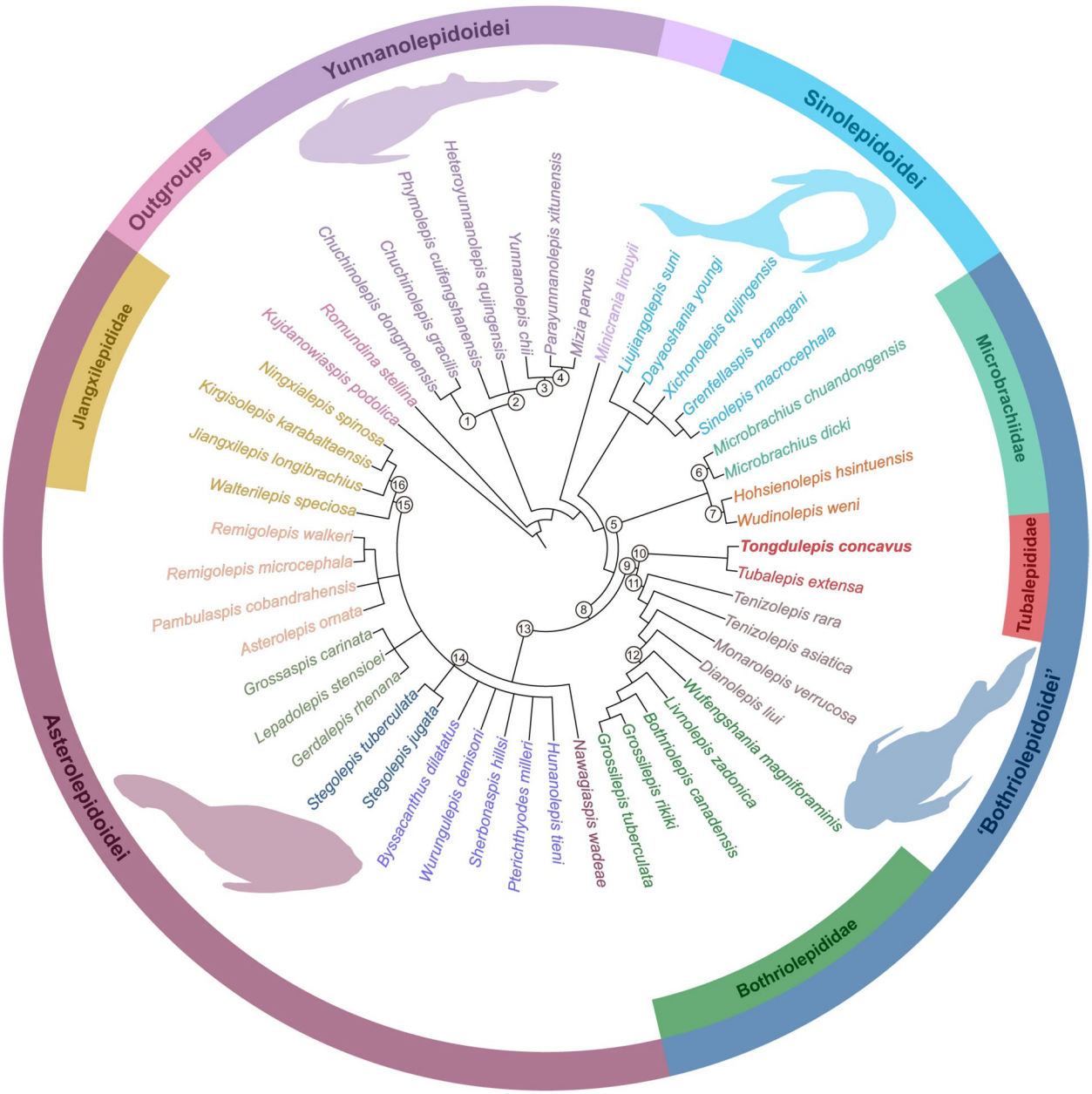

Fig. 8 Strict consensus tree of the 20 most parsimonious trees to show the phylogenetic position of *Tongdulepis* gen. nov. within the Antiarcha. Length = 270 steps, consistency index (CI) = 0.356, retention index (RI) = 0.718

wall of trunk shield (Ch. 3, state 1); anterior median dorsal plate partly overlapping anterior dorsolateral plate (Ch. 53, state 1); presence of brachial process (Ch. 72, state 1); postmarginal plate posterolateral of paranuchal plate (Ch. 82, state 1). *Wudinolepis* and *Hohsienolepis* form a monophyletic group (Node 7, Fig. 8), characterized by their fused posterior ventrolateral and posterior lateral plates (Ch.65, state 1).

The remaining euantiarchs (Node 8, Fig. 8) are supported by three synapomorphies: absence of the preorbital depression (Ch. 13, state 0); short and broad postpineal and nuchal plates (Ch. 21, state 1); supraotic thickening on the visceral view of nuchal plate (Ch. 25, state 1). The main branch of the 'Bothriolepidoidei' comprises the *Tubalepis-Tenizolepis-Dianolepis-Bothriolepis* clade (Node 9, Fig. 8), characterized by four synapomorphies: preorbital recess extending laterally to the

lateral plates (Ch. 16, state 1); postorbital crista extending obliquely to nuchal plate (Ch. 23, state 1); elongated pectoral appendage (Ch. 77, state 1); elongated lateral marginal plate 2 (Ch. 78, state 1).

Tongdulepis gen. nov. is placed as the sister taxon of *Tubalepis* within Tubalepididae (Node 10, Fig. 8), defined by the absence of the postmarginal plate (Ch. 81, state 0). Tubalepididae is suggested as a diverging group in Bothriolepidoidei (Miles, 1968), and is plesiomorphic of the *Tenizolepis-Dianolepis-Bothriolepis* lineage (Node 11, Fig. 8), which is further supported by anterior median dorsal plate completely overlapping anterior dorsolateral plate (Ch. 53, state 0), and ventral tuberosity on posterior median dorsal plate (Ch. 86, state 1). Dianolepididae is paraphyletic in our result, and Bothriolepididae (Node 12, Fig. 8) is characterized by two synapomorphies including a nuchal plate with orbital facets (Ch. 24, state 1), and a branch of infraorbital canal diverging on the lateral plate (Ch. 32, state 1).

Nawagiaspis was previously referred to as the nearest sister group to Asterolepidoidei (Zhu, 1996), a bothriolepidoid (Jia et al., 2010), or an asterolepidoid (Plax & Lukševičs, 2023; Wang & Zhu, 2018). Our research supports *Nawagiaspis* at the most basal position of the asterolepidoid lineage (Node 13, Fig. 8). *Nawagiaspis* is united with other asterolepidoids by three synapomorphies: narrow lateral plate (Ch. 12, state 0); high and short trunk shield (Ch. 47, state 1); index between the width of the anterior margin and maximum width of anterior median dorsal plate between 35 to 55 (Ch. 49, state 1). The main asterolepidoid lineage (Node 14, Fig. 8) is characterized by five synapomorphies: occipital cross-commissure long and extending onto nuchal plate (Ch. 34, state 1); absence of submarginal articulation (Ch.42, state 0); absence of postsuborbital plate (Ch. 43, state 0); centrally or posteriorly placed tergal angle of anterior median dorsal plate (Ch. 51, state 0); absence of anterior ventral process and pit on anterior median dorsal plate (Ch.56, state 0).

Zhang and Liu (1991) established Jiangxilepidae in the bothriolepidoid lineage, mainly for the anterior median dorsal plate with broad anterior margin and median spine, jointed and elongated pectoral fins. Jia et al. (2010) redefined Jiangxilepididae but retained it in the bothriolepidoids. Our result assigns Jiangxilepididae to the asterolepidoid lineage, in accordance with Wang and Zhu (2018). *Jiangxilepis*, *Ningxialepis* and *Kirgisolepis* form a monophyletic group (Node 16, Fig. 8), characterized by four synapomorphies: dorsal spine of anterior median dorsal plate (Ch. 52, state 1); small axillary foramen (Ch. 74, state 0); elongated pectoral appendage (Ch. 77, state 1); elongated lateral marginal plate 2 (Ch. 78, state 1). *Walterilepis* is assigned to Jiangxilepidae (Node 15, Fig. 8) for their reticular ornamentation (Ch. 1, state 1), but the material is highly fragmented, here we hold our reservation for considering it as a member of Jiangxilepidae.

Comparison within Bothriolepidoidei

Skull roof—Moloshnikov (2011) established the family Tubalepididae because the PNu plate of *Tubalepis* lacked the anterolateral margin for connecting with the postmarginal plate (PM, Fig. 7). He suggested that *Tubalepis* may have lost its PM plate. However, some Chinese taxa, like *Liujianglepis* (Wang, 1987) and *Hohsienolepis* (P'an & Wang, 1978; Pan, 1984), were described as lacking the PM plate, possibly due to fusion in an expanded L plate. The shape of the PNu plate in *Tongdulepis* gen. nov. suggests that the PM plate is lost, and not resulting from fusion.

Microbrachiidae has been suggested as the most basal group of the euantiarchs due to possessing a preorbital depression (pr.d, Fig. 7A; Pan et al., 2018; Wang & Zhu, 2018; Zhu, 1996). In our phylogenetic analysis, Microbrachiidae is also plesiomorphic and closely related to the Tubalepididae lineage. Ignoring the PM plate in *Microbrachius* (Fig. 7A), its PNu plate is almost the same shape as that of Tubalepididae, lacking the anterolateral margin. Meanwhile, the *Tenizolepis-Dianolepis-Bothriolepis* lineage inherits the topological relationship between the PM, PNu, and L plates. The relative location of those plates is unchanged, and the preobstantic corners are always on the PM plate (Fig. 7). Our phylogeny analysis also suggests two directions of evolution, the Tubalepididae lineage forming a sister group with the *Tenizolepis-Dianolepis-Bothriolepis* lineage (Fig. 8).

As mentioned before, the orbital fenestra is wide and occupies two-thirds of the width of the head shield (Figs. 4, 6). Although the pineal plate is not preserved, the wide orbital fenestra might indicate widespread eyeballs, perhaps with a broader horizon visual field than antiarchs with smaller orbital fenestrae. Researchers suggest the large orbital fenestra is plesiomorphic, which may be a coincidence for a similar habitat (not fully benthic but with some cruising capability) between the outgroup taxa and *Tongdulepis*.

Trunk armor—Besides the notable pattern of the head shield, interesting features on the trunk armor of Tubalepididae also separate it from other Bothriolepidoidei. The dorsolateral and dorsal median ridges are absent in the tubalepids, and unlike the round trunk armor in other antiarchs, the tubalepids had elongated and slimmer trunk shields according to Moloshnikov (2011). Those features may indicate the trunk armor was drop-shaped, this may have reduced the water drag.

Brachial process—The development of the brachial process is one of the key innovations in evolution of the

antiarchs (Young & Zhang, 1992). Compared with the basal groups, the helmet-shaped articulation in the euantiarchs increased the flexibility of the pectoral appendages. The well-developed helmet-shaped articulation in *Tongdulepis* gen. nov. is distinguished from *Bothriolepis* by the dorsal and ventral articular depressions being less curved, perhaps indicating less capacity for rotation. The insertion area for the abductor muscle controlling protraction of the pectoral appendages in bothriolepids (Young, 1988) is absent in *Tongdulepis* gen. nov., suggesting weaker protraction than the bothriolepids.

The vertical flexibility of the pectoral appendage is limited by the articulation between the CD_1, CV_1, and pedal parts (Figs. 3, 6). The rotation angle in *Tongdulepis* gen. nov. is less than the horizon protracted angle (Béchard et al., 2014). The pedal part of *Tongdulepis* gen. nov. tilts downside and marks the pectoral appendages pointing more downwards, and most antiarchs have horizon-placed pectoral appendages. Moreover, the large axillary foramen posterior of the brachial process (Fig. 6) accommodates thicker nerves and vessels (e.g., the subclavian artery and vein; Young, 2008), suggesting that *Tongdulepis* gen. nov. tends to have stronger pectoral appendages than other antiarchs. The robust and more downwards pectoral appendages of *Tongdulepis* gen. nov. may help it maintain stability while cruising.

Conclusions

A new tubalepid antiarch, *Tongdulepis concavus*, is described from the Middle Devonian (Qujing Formation, late Eifelian) of Huize County. It resembles *Tubalepis* in similar tubercular ornamentation, skull roof pattern, the shape of the AMD plate, and elongated trunk armor. *Tongdulepis* gen. nov. confirms the loss of the PM plates in Tubalepididae and provides new information on the neurocranium and brachial process in basal bothriolepidoids. The wide and narrow orbital fenestra, ridge-less trunk armor, extreme concave posterior overlap on AMD plate, and large axillary foramen, confirm *Tongdulepis* gen. nov. as a distinctive taxon among bothriolepidoids. Phylogenetic analysis using a large matrix supports *Tongdulepis* gen. nov. as a member of Tubalepididae, which is more plesiomorphic than the *Tenizolepis-Dianolepis-Bothriolepis* lineage within the Bothriolepidoidei.

Abbreviations

IVPP	Institute of Vertebrate Paleontology and Paleoanthropology, Chinese Academy of Sciences, Beijing, China
Ch.	Chuandong formation
Em.	Emsian
Fm.	Formation
Sh.	Shangshuanghe formation
ad_1	Anterior articular process on submarginal plate
ADL	Anterior dorsolateral plate
a.fac	Auxiliary articular facet for pectoral appendage
a.inf	Ventral muscle insertion
alc	Anterolateral angle of head shield
alr	Postlevator thickening of anterior median dorsal plate
AMD	Anterior median dorsal plate
a.PrL	Attachment area for prelateral plate
art.d	Dorsal articular depression for dermal process of pectoral appendage
art.v	Ventral articular depression for dermal process of pectoral appendage
a_1SM	Anterior attachment area for submarginal plate
a_2SM	Posterior attachment area for submarginal plate
a.sup	Anterior dorsal muscle insertion on brachial process
a.un	Unornamented area beneath articular fossa of pectoral
AVL	Anterior ventrolateral plate
Cd_{1-3}	Dorsal central plate 1–3
cf.ADL	Area overlapping anterior dorsolateral plate
cf.MxL	Area overlapping mixilateral plate
c.nv	Canal for nerves and/or vessels
cr.im	Inframarginal crista of head shield
cr_1	Prelateral crista of transverse lateral groove of head shield
cr_2	Posterolateral crista of transverse lateral groove of head shield
cr.po	Postorbital crista
cr.tv	Transverse nuchal crista
Cv_{1-2}	Ventral central plate 1–2
dsc	Depression caused by semicircular canal
dlg_2	Posterior oblique dorsal sensory line groove
dma	Tergal angle of trunk armor
dmr	Dorsal median ridge of trunk armor
f.ax	Axillary foramen of anterior ventrolateral plate
fe.orb	Orbital fenestra
fp	Funnel pit of brachial process
f.retr	Levator fossa of anterior median dorsal plate
ifc_1	Principal section of infraorbital sensory line on head shield
ifc_2	Branch of infraorbital sensory line diverging on lateral plate
L	Lateral plate
Lc	Lateral corner of anterior median dorsal plate
lcg	Main lateral line groove
Ml_{1-4}	Lateral marginal plate 1–4
Mm_{1-2}	Mesial marginal plate 1–2
mr	Median ridge of postpineal plate
MV	Median ventral plate
MxL	Mixilateral plate
nm	Obtected nuchal area of head shield
nprl	Prelateral notch of head shield
Nu	Nuchal plate
oa.ADL	Area overlapped by anterior dorsolateral plate
oa.AMD	Area overlapped by anterior median dorsal plate
oa.PMD	Area overlapped by posterior median dorsal plate
oa.PNu	Area overlapped by paranuchal plate
occ	Occipital cross commissure
ood	Otico-occipital depression of head shield
p	Lateral pit of head shield
p.apo	Anterior postorbital process
pbr	Brachial process
pe	Pedal part of brachial process
PMD	Posterior median dorsal plate
pnt	Paranuchal trochlea
PNu	Paranuchal plate
PP	Postpineal plate
pp	Posterior pit line groove
pr.d	Preorbital depression of head shield
prh	Preorbital recess of head shield
pro	Obstantic process of trunk armor
proc	Preobstantic corner of head shield;
PrM	Premedian plate
p.sup	Posterior dorsal muscle insertion
pt_1	Anterior ventral pit of dorsal wall of trunk armor
ptoc	Postobstantic corner of paranuchal plate
PVL	Posterior ventrolateral plate

sar	Supra-articular ridge
soa	Subobstantic area of head shield
soc	Anterior section of supraorbital sensory line on premedian plate
sot	Supraotic thickening of head shield
SM	Submarginal plate
Sm	Semilunar plate
tal	Anterolateral thickening of lateral plate
tlg	Transverse lateral groove of head shield

Supplementary Information

The online version contains supplementary material available at https://doi.org/10.1186/s13358-025-00349-6.

Supplementary material 1.

Supplementary material 2.

Acknowledgements
We thank Xindong Cui and Yingtian Zhao for their help during the fieldwork, Wei Gao for taking photos, and Xiufen Lu for the specimen preparation. We further thank Gavin Young and the anonymous reviewers of the manuscript for their constructive comments and the editors for the handling of the manuscript.

Author contributions
MZ and YL organized the fieldwork. YL conducted the fieldwork, reconstructed the model, drew the figures, and wrote the manuscript. YL and MZ compiled the character matrix and performed the phylogenetic analyses. MZ and ZP contributed interpretation of the results, discussion and figures. All authors approved the final version of the manuscript.

Funding
This work was supported by the National Natural Science Foundation of China (42130209, 92255301, 42362001), and the Youth Innovation Promotion Association CAS (2021070).

Availability of data and materials
No datasets were generated or analysed during the current study.

Declarations

Competing interests
The authors declare no competing interests.

Received: 18 October 2024 Accepted: 13 January 2025
Published online: 05 March 2025

References

Béchard, I., Arsenault, F., Cloutier, R., & Kerr, J. (2014). The Devonian placoderm fish *Bothriolepis canadensis* revisited with three-dimensional digital imagery. *Palaeontologia Electronica, 17*(1), 1–19.
Brazeau, M. D. (2009). The braincase and jaws of a Devonian 'acanthodian' and modern gnathostome origins. *Nature, 457*, 305–308. https://doi.org/10.1038/nature07436
Carr, R. K., Johanson, Z., & Ritchie, A. (2009). The phyllolepid placoderm *Cowralepis mclachlani*: Insights into the evolution of feeding mechanisms in jawed vertebrates. *Journal of Morphology, 270*(7), 775–804. https://doi.org/10.1002/jmor.10719
Cope, E. D. (1885). The position of *Pterichthys* in the system. *American Naturalist, 19*(3), 289–291.
Denison, R. (1978). Placodermi. In H. P. Schultze (Ed.), *Handbook of Paleoichthyology*. Gustav Fischer Verlag. Stuttgart.
Downs, J. P., Daeschler, E. B., Lo, N., Carey, E. N., & Shubin, N. H. (2019). *Asterolepis alticristata* n. sp. (Antiarchi) from the Upper Devonian (Frasnian) of Nunavut, Canada, and a report on the antiarch diversity of the Fram Formation. *Geodiversitas, 41*(1), 679–698.
Dupret, V. (2010). Revision of the genus *Kujdanowiaspis* Stensiö, 1942 (Placodermi, Arthrodira, "Actinolepida") from the Lower Devonian of Podolia (Ukraine). *Geodiversitas, 32*(1), 5–63. https://doi.org/10.5252/g2010n1a1
Dupret, V., Sanchez, S., Goujet, D., & Ahlberg, P. E. (2017). The internal cranial anatomy of *Romundina stellina* Ørvig, 1975 (Vertebrata, Placodermi, Acanthothoraci) and the origin of jawed vertebrates - anatomical atlas of a primitive gnathostome. *PLoS ONE, 12*(2), e0171241. https://doi.org/10.1371/journal.pone.0171241
Goloboff, P. A., & Catalano, S. A. (2016). TNT version 1.5, including a full implementation of phylogenetic morphometrics. *Cladistics, 32*(2016), 221–238. https://doi.org/10.1111/cla.12160
Goujet, D. F., & Young, G. C. (1995). Interrelationships of placoderms revisited. *Geobios Mémoire Spécial, 19*, 89–95.
Goujet, D. F., & Young, G. C. (2004). Placoderm anatomy and phylogeny: New insights. In G. Arratia, M. V. H. Wilson, & R. Cloutier (Eds.), *Recent Advancesin the Origin and Early Radiation of Vertebrates* (pp. 109–126). Verlag Dr. Friedrich Pfeil. München.
Hemmings, S. K. (1978). The Old Red Sandstone antiarchs of Scotland: *Pterichthyodes* and *Microbrachius*. *Monographs of the Palaeontographical Society, 131*, 1–64.
Janvier, P. (1995). The brachial articulation and pectoral fin in antiarchs (Placodermi). *Bulletin du Muséum National d'Histoire Naturelle, Paris, 17*, 143–161.
Janvier, P., & Pan, J. (1982). *Hyrcanaspis bliecki* n. g. n. sp., a new primitive euantiarch (Antiarcha, Placodermi) from the Middle Devonian of northeastern Iran, with a discussion on antiarch phylogeny. *Neues Jahrbuch für Geologie und Paläontologie. Abhandlungen, 164*(3), 364–392.
Jia, L. T., Zhu, M., & Zhao, W. J. (2010). A new antiarch fish from the Upper Devonian Zhongning Formation of Ningxia. *China. Palaeoworld, 19*(1–2), 136–145. https://doi.org/10.1016/j.palwor.2010.02.002
Long, J. A., Mark-Kurik, E., Johanson, Z., Lee, M. S., Young, G. C., Zhu, M., Ahlberg, P. E., Newman, M., Jones, R., Den Blaauwen, J. L., Choo, B., & Trinajstic, K. (2015). Copulation in antiarch placoderms and the origin of gnathostome internal fertilization. *Nature, 517*, 196–199. https://doi.org/10.1038/nature13825
Lukševičs, E. (1991). Bothriolepids from the Ketleri Formation of the Upper Devonian of Latvia (Pisces, Placodermi). *Daba Un Muzejs, 3*, 38–50.
Lukševičs, E. (2001). Bothriolepid antiarchs (Vertebrata, Placodermi) from the Devonian of the north-western part of the East European Platform. *Geodiversitas, 23*(4), 489–609.
Luo, Y. C., Cui, X. D., Qiao, T., & Zhu, M. (2022). A new dipnoan genus from the Middle Devonian of Huize, Yunnan, China. *Journal of Systematic Palaeontology, 19*(18), 1303–1315.
Luo, Y. C., Zhu, M., & Lu, L. W. (2023). Reappraisal of *Bothriolepis sinensis* Chi, 1940 from the Tiaomachien Formation, Hunan, China. *Vertebrata PalAsiatica, 61*(4), 261–276.
Maddison, W. P., & Maddison, D. R. (2019). Mesquite: a modular system for evolutionary analysis. Version 3.61 http://mesquiteproject.org.
Malinovskaya, S. (1973). A new Middle Devonian genus *Stegolepis* (Antiarchi, Placodermi) from central Kazakhstan. *Paleontologicheskii Zhurnal, 1973*(2), 71–82.
McCoy, F. (1848). On some new fossil fish of the Carboniferous Period. *Annals and Magazine of Natural History, 2*(2), 115–133.
Miles, R. S. (1968). The Old Red Sandstone antiarchs of Scotland: Family Bothriolepididae. *Palaeontographical Society Monographs, 122*, 1–130.
Moloshnikov, S. V. (2004). Crested antiarch *Bothriolepis zadonica* H.D. Obrucheva from the lower Famennian of Central European Russia. *Acta Palaeontologica Polonica, 49*(1), 135–146.
Moloshnikov, S. V. (2008). Devonian antiarchs (Pisces, Antiarchi) from central and Southern European Russia. *Paleontological Journal, 42*(7), 691–773. https://doi.org/10.1134/s0031030108070010
Moloshnikov, S. V. (2010). A new find of the placoderm genus *Bothriolepis* Eichwald in the Upper Devonian of Uzbekistan. *Paleontological Journal, 44*(1), 79–83. https://doi.org/10.1134/s0031030110010107
Moloshnikov, S. V. (2011). Bothriolepiform antiarchs (Pisces, Placodermi) from the Devonian of Central Kazakhstan. *Paleontological Journal, 45*(3), 291–304. https://doi.org/10.1134/s0031030111030099
Moloshnikov, S. V. (2012). Middle-Late Devonian placoderms (Pisces: Antiarchi) from Central and Northern Asia. *Paleontological Journal, 46*(10), 1097–1196. https://doi.org/10.1134/s0031030112100012

Newman, M., den Blaauwen, J., & Leather, D. (2019). The antiarch fish *Asterolepis orcadensis* from the Scottish Middle Devonian. *Palaeontologia Electronica, 22*(2), 1–24.
Olive, S. (2015). Devonian antiarch placoderms from Belgium revisited. *Acta Palaeontologica Polonica, 60*(3), 711–731.
P'an, K., & Wang, S. T. (1978). Devonian Agnatha and Pisces of South China. In Institute of Geology and Mineral Resources (Ed.), Symposium on the Devonian System of South China (pp. 298–333). Geological Press, Beijing.
Pan, J. (1984). A new species of *Microbrachius* from Middle Devonian of Yunnan. *Vertebrata PalAsiatica, 22*, 9–13.
Pan, Z. H., Zhu, M., Zhu, Y. A., & Jia, L. T. (2018). A new antiarch placoderm from the Emsian (Early Devonian) of Wuding, Yunnan, China. *Alcheringa, 42*, 10–21. https://doi.org/10.1080/03115518.2017.1338357
Panteleyev, N. (1992). New remigolepids and high armoured antiarchs of Kirgizia. In E. Mark-Kurik (Ed.), *Fossil Fishes as Living Animals* (pp. 185–192). Academy of Sciences of Estonia, Academia 1.
Panteleyev, N. (1993). New antiarchs (Placodermi) from Middle Devonian sediments of Central Kazakhstan. *Paleontologicheskii Zhurnal, 1993*(2), 62–71.
Panteleyev, N. (2001). *Tubalepis extensa* (Sergienko, 1961) (Placodermi, Antiarchi) from the Upper Devonian of Minusa Depression, Southern Siberia, Russia. In Obruchev Symposium on Evolutionary Palaeoichthyology. Paleontol. Inst. RAS, Moscow. 40.
Panteleyev, N., & Moloshnikov, S. V. (2003). *Tubalepis* gen. nov. (Placodermi, Antiarchi) from the Upper Devonian of the Minusa Depression. *Paleontological Journal, 37*(4), 413–416.
Plax, D. P., & Lukševičs, E. (2023). A new Early Devonian antiarch placoderm from Belarus, and the phylogeny of Asterolepidoidei. *Acta Palaeontologica Polonica, 68*(3), 513–527.
Qiao, T., King, B., Long, J. A., Ahlberg, P. E., & Zhu, M. (2016). Early gnathostome phylogeny revisited: Multiple method consensus. *PLoS ONE, 11*(9), e0163157. https://doi.org/10.1371/journal.pone.0163157
Ritchie, A., Wang, S. T., Young, G. C., & Zhang, G. R. (1992). The Sinolepidae, a family of antiarchs (placoderm fishes) from the Devonian of South China and eastern Australia. *Records of the Australian Museum, 44*(3), 319–370. https://doi.org/10.3853/j.0067-1975.44.1992.38
Sergienko, A. (1961). A new species, *Bothriolepis extensa* sp. n., from the Tuba Formation of the Minusa depression. *Tr Sib Nauchlssled Inst Geol Geofiz Miner Syr (Data on Paleontology and Stratigraphy of Western Siberia), 15*, 139–140.
Stensiö, E. A. (1942). On the snout of arthrodires. *Kungliga Svenska Vetenskapsakademiens Handlingar, 20*(3), 1–32.
Stensiö, E. A. (1948). On the Placodermi of the Upper Devonian of East Greenland. II. Antiarchi: Subfamily Bothriolepinae. With an attempt at a revision of the previously described species of that family. *Meddelelser Om Grønland, 139*, 1–622.
Wang, J. Q., & Zhang, G. R. (1999). New material of *Microbrachius* from Lower Devonian of Qujing, Yunnan, China. *Vertebrata PalAsiatica, 37*(3), 200–211.
Wang, S. T. (1987). A new antiarch from the Early Devonian of Guangxi. *Vertebrata PalAsiatica, 25*, 81–90.
Wang, Y. J., & Zhu, M. (2018). Redescription of *Phymolepis cuifengshanensis* (Antiarcha: Yunnanolepididae) using high-resolution computed tomography and new insights into anatomical details of the endocranium in antiarchs. *PeerJ, 6*, e4808.
Young, G. C. (1983). A new antiarchan fish (Placodermi) from the Late Devonian of southeastern Australia. *BMR Journal of Australian Geology & Geophysics, 8*, 71–81.
Young, G. C. (1984a). An asterolepidoid antiarch (placoderm fish) from the Early Devonian of the Georgina Basin, central Australia. *Alcheringa, 8*, 65–80.
Young, G. C. (1984b). Comments on the phylogeny and biogeography of antiarchs (Devonian placoderm fishes), and the use of fossils in biogeography. *Proceedings of the Linnean Society of New South Wales, 107*(3), 443–473.
Young, G. C. (1984c). Reconstruction of the jaws and braincase in the Devonian placoderm fish *Bothriolepis*. *Palaeontology, 27*(3), 635–661.
Young, G. C. (1988). Antiarchs (placoderm fishes) from the Devonian Aztec Siltstone, southern Victoria Land. *Antarctica. Palaeontographica Abt. A, 202*, 1–125.
Young, G. C. (1990). New antiarchs (Devonian placoderm fishes) from Queensland, with comments on placoderm phylogeny and biogeography. *Memoirs of the Queensland Museum, 28*(1), 35–50.
Young, G. C. (2008). The relationships of antiarchs (Devonian placoderm fishes) - evidence supporting placoderm monophyly. *Journal of Vertebrate Paleontology, 28*(3), 626–636.
Young, G. C. (2010). Placoderms (armored fish): Dominant vertebrates of the Devonian period. *Annual Review of Earth and Planetary Sciences, 38*(1), 523–550.
Young, G. C., & Gorter, J. D. (1981). A new fish fauna of Middle Devonian age from the Taemas/Wee Jasper region of New South Wales. *Bulletin of the Bureau of Mineral Resources Geology and Geophysics Australia, 209*, 85–147.
Young, G. C., & Zhang, G. R. (1992). Structure and function of the pectoral joint and operculum in antiarchs. Devonian Placoderm Fishes. *Palaeontology, 35*(2), 443–464.
Young, G. C., & Zhang, G. R. (1996). New information on the morphology of yunnanolepid antiarchs (placoderm fishes) from the Early Devonian of South China. *Journal of Vertebrate Paleontology, 16*(4), 623–641.
Zhang, G. R. (1965). New antiarchs from the Middle Devonian of Yunnan. *Vertebrata PalAsiatica, 9*(1), 1–9.
Zhang, G. R., & Liu, Y. H. (1991). A new antiarch from the Upper Devonian of Jiangxi, China. In M. M. Chang, Y. H. Liu, & G. R. Zhang (Eds.), *Early Vertebratesand Related Problems of Evolutionary Biology* (pp. 195–212). Science Press. Beijing.
Zhang, G. R., & Young, G. C. (1992). A new antiarch (placoderm fish) from the Early Devonian of South China. *Alcheringa, 16*, 219–240.
Zhang, M. M. (1980). Preliminary note on a Lower Devonian antiarch from Yunnan. *China. Vertebrata PalAsiatica, 18*(3), 179–190.
Zhu, M. (1996). The phylogeny of the Antiarcha (Placodermi, Pisces), with the description of Early Devonian antiarchs from Qujing, Yunnan, China. *Bulletin du Muséum National d'Histoire Naturelle, 18*, 233–347.
Zhu, M., Yu, X. B., Ahlberg, P. E., Choo, B., Lu, J. T., Qiao, T., Qu, Q. Y., Zhao, W. J., Jia, L. T., Blom, H., & Zhu, Y. A. (2013). A Silurian placoderm with osteichthyan-like marginal jaw bones. *Nature, 502*(7470), 188–193. https://doi.org/10.1038/nature12617
Zhu, Y. A., Giles, S., Young, G. C., Hu, Y. Z., Bazzi, M., Ahlberg, P. E., Zhu, M., & Lu, J. (2021). Endocast and bony labyrinth of a Devonian "placoderm" challenges stem gnathostome phylogeny. *Current Biology, 31*(5), 1112–1118. https://doi.org/10.1016/j.cub.2020.12.046
Zhu, Y. A., Li, Q., Lu, J., Chen, Y., Wang, J. H., Gai, Z. K., Zhao, W. J., Wei, G. B., Yu, Y. L., Ahlberg, P. E., & Zhu, M. (2022). The oldest complete jawed vertebrates from the early Silurian of China. *Nature, 609*(7929), 954–958. https://doi.org/10.1038/s41586-022-05136-8

Publisher's Note